Nucleic Acids Research Advance Access published September 8, 2015

Nucleic Acids Research, 2015 **1**
doi: 10.1093/nar/gkv875

Sequence-specific recognition of DNA minor groove by an NIR-fluorescence switch-on probe and its potential applications

Nagarjun Narayanaswamy[1], Shubhajit Das[2], Pralok K. Samanta[3], Khadija Banu[4], Guru Prasad Sharma[5], Neelima Mondal[5], Suman K. Dhar[4], Swapan K. Pati[2,3] and T. Govindaraju[1,*]

[1]Bioorganic Chemistry Laboratory, New Chemistry Unit, Jawaharlal Nehru Centre for Advanced Scientific Research, Jakkur P.O., Bengaluru 560064, India, [2]New Chemistry Unit, Jawaharlal Nehru Centre for Advanced Scientific Research, Jakkur P.O., Bengaluru 560064, Karnataka, India, [3]Theoretical Sciences Unit, Jawaharlal Nehru Centre for Advanced Scientific Research, Jakkur P.O., Bengaluru 560064, Karnataka, India, [4]Special Centre for Molecular Medicine, Jawaharlal Nehru University, New Delhi, India and [5]School of Life Sciences, Jawaharlal Nehru University, New Delhi, India

Received June 26, 2015; Revised August 12, 2015; Accepted August 19, 2015

ABSTRACT

In molecular biology, understanding the functional and structural aspects of DNA requires sequence-specific DNA binding probes. Especially, sequence-specific fluorescence probes offer the advantage of real-time monitoring of the conformational and structural reorganization of DNA in living cells. Herein, we designed a new class of D2A (one-donor-two-acceptor) near-infrared (NIR) fluorescence switch-on probe named quinone cyanine–dithiazole (QCy–DT) based on the distinctive internal charge transfer (ICT) process for minor groove recognition of AT-rich DNA. Interestingly, QCy–DT exhibited strong NIR-fluorescence enhancement in the presence of AT-rich DNA compared to GC-rich and single-stranded DNAs. We show sequence-specific minor groove recognition of QCy–DT for DNA containing 5′-AATT-3′ sequence over other variable (A/T)4 sequences and local nucleobase variation study around the 5′-*X*(AATT)*Y*-3′ recognition sequence revealed that *X* = A and *Y* = T are the most preferable nucleobases. The live cell imaging studies confirmed mammalian cell permeability, low-toxicity and selective staining capacity of nuclear DNA without requiring RNase treatment. Further, *Plasmodium falciparum* with an AT-rich genome showed specific uptake with a reasonably low IC_{50} value (<4 μM). The ease of synthesis, large Stokes shift, sequence-specific DNA minor groove recognition with switch-on NIR-fluorescence, photostability and parasite staining with low IC_{50} make QCy–DT a potential and commercially viable DNA probe.

INTRODUCTION

Sequence-specific recognition is an essential criterion to target and control DNA functions for gene-expression, bioimaging, diagnostics, therapeutics and biotechnological applications (1,2). Over the years, many probes have been developed to target DNA, but there is still a pressing need for developing efficient new probes and therapeutic agents against gene-related diseases as DNA remains a promising biological receptor (3–6). It is a daunting task indeed to design site-specific DNA binding molecules with high affinity and selectivity. To achieve this goal, base-pair and sequence-selective DNA binding probes ranging from small molecules to large peptides of natural and synthetic origin have been developed (7–11). These probes interact with DNA mainly through two binding modes, intercalation and groove binding. Typically, small molecules binding to DNA through intercalation possess the site-specificity of three base pairs that can differentiate only one out of 32 random sequences (12). Factually, the human genome contains 3 billion base pairs and the small molecular probe is posed with the astonishingly large number of 1 billion unique binding sites (13). To improve the binding specificity of small molecular probes over longer DNA sequences, researchers shifted their attention toward groove-binding agents. DNA grooves are sites with inherent hydrogen bond donors and accep-

*To whom correspondence should be addressed. Tel: +918022082969; Fax: +918022082627; Email: tgraju@jncasr.ac.in
Present address: T. Govindaraju, Bioorganic Chemistry Laboratory, New Chemistry Unit, Jawaharlal Nehru Centre for Advanced Scientific Research, Jakkur P.O., Bengaluru 560064, Karnataka, India.

tors at the edges of nucleobases, which makes them adaptable to recognition through hydrogen bonding interactions in a sequence-selective manner (10,11,14–16). In comparison with DNA major groove, the minor groove is narrow in size, which makes it suitable for small molecular probes. In particular, sequence-specific targeting of DNA using minor groove-binding molecules is considered a promising molecular recognition strategy in chemistry and biology (10,11,14–16).

Dervan and co-workers developed sequence-specific N-methylpyrrole and N-methylimidazole-containing crescent-shaped polyamides that can selectively recognize and bind DNA minor grooves through hydrogen bonding interactions (9,11,13–16). These polyamides are one of the most elegantly designed molecules to recognize the minor groove of DNA with superior discrimination of all four Watson-Crick base pairs (13). However, their difficult synthesis processes and non-fluorescent nature eventually limited their potential applications in biological systems. Recently, polyamide/fluorophore conjugates have been developed and their cellular uptake properties studied in various cell lines (15,16). Later, Wilson *et al*. reported phenylfuran-benzimidazole diamidine-based cell permeable and sequence-selective minor groove-binding molecules (6,17–21). One of the common structural features of all these minor groove-binding ligands is the molecular curvature to complement the DNA minor groove concavity, referred to as '*isohelicity,*' which enhances the binding affinity and selectivity of interaction (10,11,17–20). Recent studies show that a majority of the minor groove-binding molecules actually target AT-rich mitochondrial kinetoplast DNA of eukaryotic cells and that of the protozoan parasite *Plasmodium falciparum* (3,6,20,22,23). Such interactions induce topological changes in AT-rich DNA, which can generate biological response against certain diseases and also serve as model systems to gain insights into the structural organization of DNA (24). Minor groove binding ligands such as distamycin A, netropsin, 4′-6-diamidino-2-phenylindole (DAPI) and bis-benzimide (Hoechst 33258) have been used as antibiotics as they bind to the minor groove of B-DNA with a preference for AT-rich sequences and are considerably more toxic to parasites than to mammalian cells (3,6). Further, availability of myriad genome warrants the need for developing efficient and highly predictive molecular tools to probe its organization and functional aspects. Overall, it is clear that sequence-specific targeting of DNA is crucial for studying sequence variation, structural organization and function in the cell nucleus.

Fluorescence probes have become powerful tools in cell biology and play a vital role in the modern era of biological research (25–27). Apart from simple detection they offer the additional advantage of real-time monitoring of conformational changes and structural reorganization of biological macromolecules in living cells and organisms (25–27). In this context, structural, functional, and therapeutic study of DNA in the cell nucleus requires sequence-specific, minor groove-binding fluorescence probes (28,29). Fluorescence imaging of DNA has been widely used to stain the nuclei of live or fixed cells and study structural reorganization of chromosome in the cell nucleus (28–30). DAPI, bis-benzimides (Hoechst dyes) and propidium iodide are well-known nuclear staining agents (31). However, the blue fluorescence DNA staining probes (DAPI and Hoechst) require excitation in the ultraviolet (UV) region and the prolonged UV illumination is certain to damage cellular DNA. Additionally, propidium iodide and related dyes are intercalators suffering from poor cell-permeability and high toxicity, apart from inducing structural alterations in the target DNA structure, which prohibits their use in biological applications (31). The limitations of existing probes and the quest to develop novel probes with superior properties motivated us to design a new, sequence-specific NIR fluorescence probe for DNA. Such fluorescence DNA probe must satisfy the following properties: (i) excitation and emission in the longer wavelength region, (ii) switch-on fluorescence response, (iii) high sequence-specificity, (iv) good quantum yield, (v) non-toxicity and (vi) live-cell permeability. In recent years, NIR-fluorescence probes have been gaining considerable attention due to their broad range of *in vivo* imaging applications that avoid interference from the absorbance and auto-fluorescence of cellular components (32,33). The deep tissue penetration ability of NIR radiation makes these probes a versatile and inexpensive alternative to classical radioisotope-detection methods (32,33). Our research group is particularly interested in developing novel red- and NIR-fluorescence probes for biomolecules and toxic protein aggregates (30,34,35). Recently, we reported an AT-base pair selective, cell permeable, red-emitting thiazole-coumarin (TC) hemicyanine probe for cell-cycle analysis, selective nuclear staining and other applications (30). Probe **TC** showed preferential AT-base pair selectivity with ∼10–20 folds fluorescence enhancement, as a function of number of AT-base pairs with a moderate association constant ($K_a = 1 \times 10^5\ M^{-1}$). The intercalation mode of binding and moderate binding affinity of probe TC to DNA encouraged us to design a new high affinity, sequence-specific NIR fluorescence switch-on probe for DNA minor groove recognition.

In the present study, we report a bent-shaped molecular probe quinone cyanine–dithiazole (**QCy–DT**), a D2A (one-donor-two-acceptor) π–electron system that is designed to undergo internal charge transfer to convert itself into a switch-on NIR–fluorophore upon binding to DNA (Figure 1). The bent shaped **QCy–DT** was expected to obey *isohelicity* and recognize the minor groove of duplex DNA with switch-on NIR-fluorescence response. Remarkably, fluorescence and circular dichroism (CD) studies reveal that **QCy–DT** binding to AT-rich DNA minor groove, in fact, result in switch-on NIR-emission in a sequence-specific manner, especially with a 5′-*A*AATT*T*-3′ sequence. Most of the desirable properties such as large Stokes shift, switch-on fluorescence (non-aggregated and non-fluorescent in unbound-state but emit NIR-fluorescence in DNA bound-state), and sequence-specific binding of **QCy–DT** in buffer solution demonstrate its superiority as a DNA probe. The live cell imaging studies confirm low-toxicity, cell permeability, effective nuclear DNA staining and photostability by **QCy–DT** at low concentration (≤1 μM) without the need of RNase treatment. Uptake of **QCy–DT** by *Plasmodium* nucleus at a very low concentration of 500 nM and a low (<4 μM) inhibitory concentration (IC_{50}) against malarial parasites indicates that **QCy–DT** may have potential use

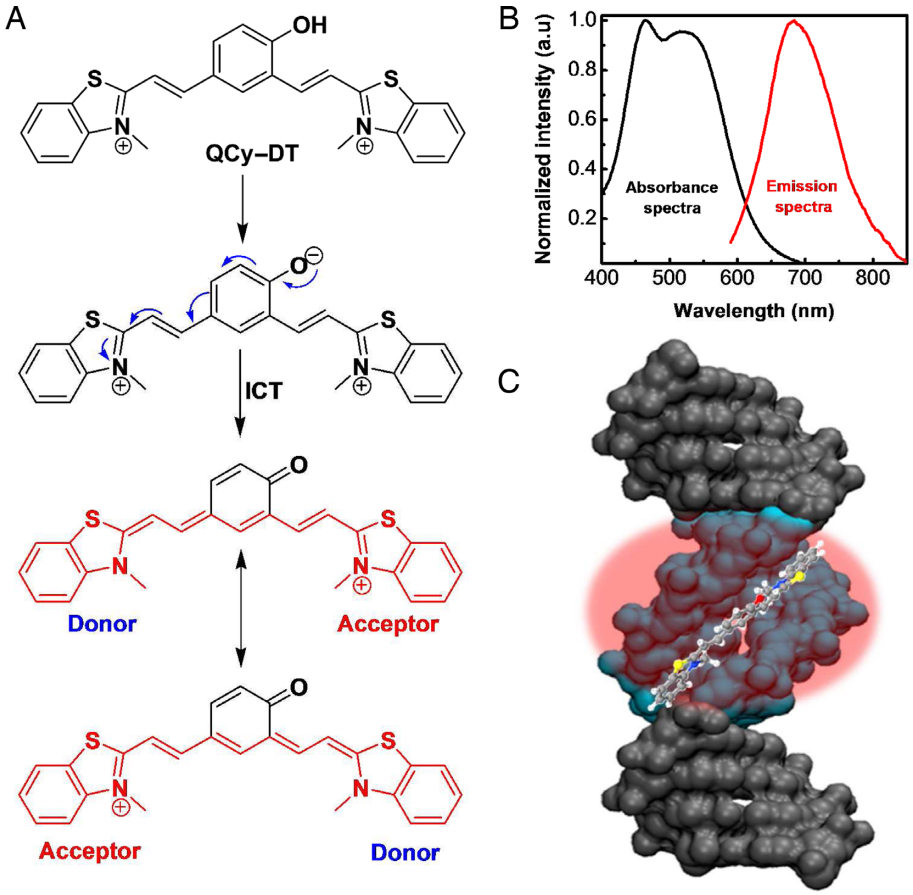

Figure 1. (**A**) Molecular structure of **QCy–DT** and activation of **QCy–DT** to form 'NIR-ready' fluorescence probe (Cy7 system). (**B**) The absorbance and emission spectra of **QCy–DT** in buffer solution (Tris-HCl, 100 mM, pH = 7.4). (**C**) DNA minor groove recognition of **QCy–DT** through switch-on NIR-fluorescence response.

against parasitic infections. To the best of our knowledge, this is the first report of a sequence-specific recognition of DNA minor groove by a switch-on NIR-fluorescence probe. **QCy–DT** displays high sequence-specificity (5′-*A*AATT*T*-3′) for DNA minor groove and is a potential probe for nuclear DNA staining of live and fixed mammalian cells, among other molecular and cell biology applications.

MATERIALS AND METHODS

General information

All the chemicals, reagents, single-stranded oligos (dA_{20}, dT_{20}, dG_{20}, dC_{20}), self-complementary oligos {$d(ATAT)_5$, $(D1)_{mix}$, Drew-AT, Calf-Thymus DNA (CT–DNA), (DM1, DM2, DM3, DM4, DM5, DM6 and DM7)}, RNA, Hoechst 33258 and Cresol Violet were purchased from Sigma–Aldrich. ^1H and ^{13}C NMR spectra were recorded on a Bruker AV-400 MHz spectrometer with chemical shifts reported as parts per million (*ppm*) (in DMSO-d_6, tetramethylsilane as an internal standard) at 20°C. UV-vis absorption and emission spectra were measured in quartz cuvettes of 1 cm path length. High resolution mass spectra (HRMS) were obtained on Agilent Technologies 6538 UHD Accurate-Mass Q-TOF LC/MS spectrometer.

Synthesis of QCy–DT

To a stirred solution of 2-methyl benzothiazole (7.0 mmol) in dichloromethane (10 ml), methyl iodide (14.0 mmol) was added dropwise and allowed to reflux overnight. Completion of the reaction was monitored by thin layer chromatography (TLC). After completion of the reaction, a white colored precipitate was formed. The precipitate was filtered and washed with copious amount of diethyl ether for removing the unreacted benzothiazole. The obtained product (N-methyl-2-methylbenzothiazole) (**1**) was dried under vacuum and used for the next reaction without further purification.

Piperidine (8 μl) was added to a stirred solution of N-methyl-2-methylbenzothiazole (**1**) (0.1 g, 0.34 mmol) in ethanol (8 ml). After 10 min, 4-hydroxyisophthalaldehyde (**2**) (20 mg, 0.14 mmol) in ethanol (2 ml) was added and the reaction mixture was stirred at 80°C for 3 h under nitrogen atmosphere. After completion of reaction, solvent was evaporated and the crude product was purified by preparative RP-HPLC (grad. 50–65% acetonitrile in water, 12 min) to obtain the probe **QCy–DT** as a yellow powder. Yield 45%. IR (neat): 3390, 3065, 3015, 1682, 1667, 1582, 1505, 1121 cm^{-1}, ^1H NMR (400 MHz, *DMSO-d*$_6$) δ_{ppm}: 8.59 (d, $J = 2$ Hz, 1 H), 8.42 (d, $J = 8.1$ Hz, 2 H), 8.30 (d, $J = 8.2$ Hz, 1 H), 8.26 (d, $J = 3.3$ Hz, 1 H), 8.23 (d, $J = 10.7$ Hz, 1 H),

8.19 (dd, $J = 2$Hz, $J = 8.7$ Hz, 1 H), 8.13 (dd, $J = 8.1$ Hz, $J = 16$ Hz, 2 H), 7.98–7.89 (m, 3 H), 7.86 (dd, $J = 1.1$ Hz, $J = 9.5$ Hz, 1 H), 7.83–7.78 (m, 2 H), 7.22 (d, $J = 8.7$ Hz, 1 H), 4.36 (s, 6 H). ^{13}C NMR (100 MHz, *DMSO-d*$_6$) δ_{ppm}: 172.1, 171.8, 161.8, 147.7, 142.2, 142.1, 142.0, 134.8, 132.6, 129.5, 128.5, 127.8, 127.6, 125.9, 124.1, 121.5, 117.7, 116.9, 116.8, 114.3, 111.8, 36.3, 36.2. HRMS (ESI-MS): found 441.1070, calcd. for $C_{26}H_{22}N_2OS_2$ $[M\text{-}2I\text{-}H]^{1+}$ m/z = 441.1095.

Sample preparation for UV-vis and fluorescence measurements

Stock solutions of **QCy–DT** were prepared in double-distilled (dd) water in the order of 10^{-3} M and stored at −10°C. DNA stock solutions were prepared by dissolving oligo samples in double-distilled (dd) water in the order of 10^{-4} M. Solutions of DNA duplexes were prepared in Tris-HCl (100 mM, pH = 7.4) buffer solution by mixing complementary DNA strands in equimolar concentration, this solution was then subjected to annealing by heating up to 85°C for 15 min., subsequently cooled to room temperature for 7 h and stored in the refrigerator (4°C) for 4 h (30).

Absorption and emission spectra

The UV-vis absorption and emission spectra were recorded on Agilent Technologies Cary series UV-vis-NIR absorbance and Cary eclipse fluorescence spectrophotometers, respectively. Thermal denaturation (UV-melting) studies were carried out on Cary 5000 UV-vis-NIR spectrophotometer equipped with Cary temperature controller in the range of 10°C to 90°C with a ramp rate of 1°C/min. The variable temperature/wavelength mode was used. Absorption was monitored at 260 nm with regular 5°C intervals. Melting temperatures (T_m) of DNA samples were calculated from the first derivatives of the absorption versus temperature curves (thermal denaturation or melting curves) obtained by monitoring at 260 nm.

Circular dichroism (CD) spectroscopy

CD measurements were carried out on Jasco J-815 spectrometer equipped with a Peltier-type temperature controller (CDF-4265/15) under a nitrogen atmosphere to avoid water condensation. Scans were performed over the range of 200–700 nm with a speed of 100 nm/min, and the spectra represent an average of three scans. A blank sample containing Tris-HCl buffer solution (100 mM, pH = 7.4) was treated in the same manner and subtracted from the collected data.

Quantum yield calculation

Cresyl violet perchlorate in ethanol ($\phi = 0.54$) was used as the standard for the fluorescence quantum yield calculation using the absorption of the test sample. The emission spectral area is obtained in the 550–800 nm regions. Dilute solutions (10^{-6} M) were used to minimize reabsorption effects of the dyes. Quantum yields were determined using the following equation,

$$\phi_s = \phi_r(\mathbf{F}_s/\mathbf{F}_r) \times (\mathbf{A}_r/\mathbf{A}_s) \times (n_s^2/n_r^2)$$

Where, ϕ_r and ϕ_s are the quantum yield of reference and sample respectively, $\mathbf{F}_r$ and $\mathbf{F}_s$ are the integrated intensities (areas) of standard and sample spectra, $\mathbf{n}_r$ and $\mathbf{n}_s$ are the refractive indices of the reference and sample solution, $\mathbf{A}_r$ and $\mathbf{A}_s$ are the absorbance intensities of reference and sample, respectively.

Fluorescence study in live cells

MCF-7 cells were propagated on 20 mm cover slips in a 6-well plate in DMEM medium supplemented with 10% fetal bovine serum at 37°C in a humidified atmosphere containing 5% CO_2 till 80% confluency was achieved. Cells were incubated for 60 min with probe **QCy–DT** (resuspended in Mili-Q water) at various concentrations (0.5 μM and 1 μM) in a humidified CO_2 incubator at 37°C. Milli-Q water was used as a vehicle control. Following the treatment, fluorescence microscopy was performed using Carl Zeiss AXIO Imager Z1 and the software used for image capturing was AxioVision Rel. 4.8.

Fluorescence study in fixed cells

HeLa cells were grown on the cover slip for 24 h in DMEM medium supplemented with 10% fetal bovine serum at 37°C in a humidified atmosphere containing 5% CO_2 till 80% confluency was achieved. Then cells were fixed with 4% paraformaldehyde in PBS for 10 min. After rinsing twice with PBS, HeLa cells were treated separately with probe **QCy–DT** at various concentrations (0.5 μM and 1 μM) for 10 min at room temperature. Subsequently, cover slips were incubated with Hoechst 33258 at 10 μg/ml for nuclear staining. Fluorescence images were taken by Carl Zeiss Laser Scanning Microscope (LSM510 META).

Plasmodium falciparum culture, synchronization and treatment of malaria parasites with probe QCy–DT

P. falciparum strain 3D7 was cultured as described previously (36). Briefly, malaria parasites were cultured in human erythrocytes in T75 flasks with RPMI 1640 (Gibco) supplemented with 10 μg/ml gentamicin (Sigma), 50 μg/ml ampicillin, 0.2% $NaHCO_3$ (Sigma), 0.5% albumax (Invitrogen) and Hypoxanthine (27 mg/l). The culture was maintained under standard conditions (37°C in 90% nitrogen, 5% CO_2 and 5% O_2). For synchronization of the parasites, ring-staged parasites were treated with 5% sorbitol at 37°C for 5–10 min, followed by washing with pre-warmed incomplete medium twice, and placed back in complete medium. **QCy–DT** probe (resuspended in Mili-Q water) was added to parasites (25 ± 2 hpi) at a final concentration of 0.5 μM and the parasites were incubated for 30 min at 37°C. Following treatment fluorescence imaging of the parasites was performed using Carl Zeiss AXIO Imager Z1 and the software used for image capturing was AxioVision Rel. 4.8.

IC_{50} determination in malaria parasites

To determine the IC_{50} value of **QCy–DT** against *P. falciparum*, parasites were synchronized in ring stage (∼12 ± 2 h) and parasitemia was maintained at ∼1%, followed by

treatment with 0, 0.5, 1, 2 and 4 μM of **QCy–DT** at early trophozoite stage (∼20 ± 2 h). After 40 h of the **QCy–DT** treatment, Geimsa stained slides were prepared, and parasitemia was counted. At least six homogenous microscopic fields were counted for each treatment, and each experiment was done in triplicates. The graphs were plotted for the percentage of parasitemia (at 0 time point and at 40 h after incubation with **QCy–DT**) against **QCy–DT** concentration, with mean and standard error.

Cell viability assay

MCF-7 cells (4×10^3 cells/well) were seeded in 96-well plate (flat bottom) and cultured for 12 h. Following this, cells were treated with 2, 4 and 8 μM of probe **QCy–DT**, respectively, for 72 h and further incubated in a humidified CO_2 incubator at 37°C. 20 μl of MTT (5 mg/ml in PBS) solution was added to each well and incubated for 4 h at 37°C in the CO_2 incubator. DMSO (200 μl) was then added to each well. After 1 h, absorbance was taken in ELISA microplate reader at 570 nm wavelength. Following formula was applied for the calculation of percentage of cell viability (CV):

$$\mathrm{CV} = \left(\frac{\text{absorbance of the experimental samples}}{\text{absorbance of the control sample}}\right) \times 100$$

The data were normalized with control and plotted with mean and standard error.

Photostability assay in MCF-7 by confocal fluorescence microscopy imaging

MCF-7 Cells were propagated on 20 mm cover slips in a 6-well plate in DMEM medium supplemented with 10% fetal bovine serum at 37°C in a humidified atmosphere containing 5% CO_2 till 80% confluency was achieved. Cells were incubated for a duration of 60 min with probe **QCy–DT** (resuspended in Mili-Q water) at 2 μM concentration in a humidified CO_2 incubator at 37°C. Following treatment, the photostability of **QCy–DT** was measured by continuous scanning using OLYMPUS FV1000 confocal fluorescence microscope, under 568 nm line of an Argon ion laser for different time durations 10 s, 120 s and 300 s. Olympus Fluoview software was used to quantitatively investigate the intensity of signals of **QCy–DT** at zero time points and after photo bleaching. The data were plotted with mean and standard error.

RESULTS AND DISCUSSION

DNA probes such as thiazole orange (TO) and oxazole yellow (YO) belong to the cyanine family, but surprisingly, no NIR-fluorescence probe with cyanine platform has been reported for DNA with sequence specificity. Cyanine dyes are composed of polymethine bridges between the N-alkylated heterocyclic aromatic groups such as pyridine, quinoline, benzoxazole and benzothiazole (37). The fluorescence property of cyanine dyes depends on complete delocalization of π-electrons between the donor-acceptor nitrogen atoms connected by polymethine bridges. Non-fluorescence in the unbound-state and strong fluorescence in the bound-state nature of most of the cyanine probes inspired us to design a cyanine-based NIR probe for DNA. In this Article, we present a one-donor-two-acceptor (D2A) quinone cyanine (QCy7) based probe **QCy–DT** designed to recognize DNA minor groove by switch-on NIR-fluorescence. Quinone cyanine (**QCy7**) fluorophore is a new class of NIR-fluorescence cyanine probes reported by Shabat *et al.* (38–40). Typically, these probes are composed of a donor phenol moiety conjugated with two heterocyclic electron acceptors such as alkylated quinolines, indolines or pyridines. **QCy–DT** was synthesized through Knoevenagel condensation of 4-hydroxyisophthalaldehyde with N-methylated benzothiazole in the presence of piperidine as a base (supplementary Scheme 1). This simple and straightforward synthesis route makes **QCy–DT** highly economical and, hence, a commercially viable probe.

As illustrated in Figure 1, deprotonation of phenol generates phenolate, which donates electrons to one of the conjugated acceptors (N-alkylated benzothiazole) and triggers internal charge transfer (ICT) to the quaternary nitrogen atom on another benzothiazole group. This ICT process results in the generation of a highly delocalized π-electron system, resembling the Cy7 fluorophore (Figure 1A). However, the protonated form of **QCy–DT** (i.e. phenol form) is non-fluorescent due to the lack of the ICT process. In order to assess the conditions for deprotonation of **QCy–DT** to generate phenolate, we performed pH-dependent fluorescence measurements in Tris-HCl solution (100 mM, pH = 7.4). Under acidic conditions (pH = 2–5), **QCy–DT** did not fluoresce, owing to a stable phenol form. Interestingly, the probe showed weak but basal NIR-fluorescence (λ_{max} = 680 nm) in the pH range of 6–8 (Supplementary Figure S1). Thus, pH-dependent fluorescence study revealed that under physiological conditions, **QCy–DT** exists mostly in the phenolate form with basal NIR-fluorescence (NIR-ready). The weak but basal fluorescent nature of **QCy–DT** (NIR-ready fluorescence probe) under physiological conditions meets our prime criterion that the probe is relatively non-fluorescent in the unbound-state but fluoresces strongly in DNA bound-state.

Photophysical properties of QCy–DT

We studied the molecular interactions of **QCy–DT** by evaluating the absorption and emission properties in Tris-buffer (100 mM, pH = 7.4) under ambient conditions. The UV-vis absorption spectra of **QCy–DT** (2 μM) exhibit two absorption maxima at 463 and 530 nm (Figure 1B) (ε = 14 950 $M^{-1}cm^{-1}$). The absorption band at 530 nm originates from the delocalization of π-electrons between phenolic oxygen and *p*-substituted benzothiazolium vinyl moiety in **QCy–DT** while the band at 463 nm is from the similar conjugation of *o*-substituted benzothiazolium vinyl moiety in **QCy–DT** (38). The absorption spectra of **QCy–DT** showed a linear increase in absorbance with increasing concentration from 0 to 8 μM (Supplementary Figure S2). This linear increase in absorbance in the range of 0 to 8 μM of **QCy–DT** suggests molecularly dissolved and non-aggregated state in buffer solution, under ambient conditions. Upon excitation at 530 nm, **QCy–DT** showed a weak but basal emission peak in the NIR region at 680 nm with a large Stokes shift ($\Delta\lambda_{max}$

= ∼150 nm) (Figure 1B). This is a very useful property as it helps avoid self-absorption in the higher energy part of emission. Furthermore, the large Stokes shift of **QCy–DT** makes it superior to many of the DNA-binding cyanine probes such as TO, YO, Picogreen, SYBR- Green I**,** cyanine dimers TOTO-1 and YOYO-1 (supplementary Table S1) (41,42). The NIR-fluorescence of **QCy–DT** arises due to extended through the Cy7 backbone and ICT process. The weak or non-fluorescent behavior of dye molecules in buffer solution is mainly attributed to the intramolecular twisting processes, which cause quenching of the fluorescence of cyanine dyes, solvation with water molecules also aids the fluorescence quenching by means of deactivation of radiative pathways (43). We believe both these processes contribute to the weak or non-fluorescent nature of **QCy–DT** in buffer solution.

Next, we performed the ground-state and excited-state calculations using density functional theory (DFT) with the PBE0 (44) functional and 6–311++G(d,p) basis set for all atoms to support our assignments of the absorption and emission bands of **QCy–DT** in water (complete computational details are given in supplementary data). DFT calculations show that the two π-π* transitions are located near 2.32 eV (S1) and 2.88 eV are in good agreement with two experimentally observed absorption bands of **QCy–DT** in buffer solution, as shown in Figure 1B. The first π-π* state is the lowest transition dominated by the HOMO to LUMO (97%) configuration while the second π-π* state is dominated by the configuration HOMO to LUMO+1 (97%). Relevant molecular orbitals for these transitions are shown in Supplementary Figure S3.

Switch-On NIR-fluorescence in the presence of DNA

The large Stokes shift, molecularly dissolved-state and non-fluorescent behavior of **QCy–DT** in buffer solution prompted us to assess its recognition ability of DNA. For this, we chose poly AT-duplexes such as $(A\text{-}T)_{20}$, self-complementary $d(ATAT)_5$, Drew-AT (14 base pair self-complementary sequence with 6AT-base pairs in central core) (45), poly GC-duplex $(G\text{-}C)_{20}$, $(D1)_{mix}$, which is a 16 base pair long self-complementary duplex and CT-DNA as mixed AT/GC duplexes (supplementary Table S2). In the presence of Drew-AT, **QCy–DT** (2 μM) showed prominent red-shifted ($\Delta\lambda_{max}$ = ∼34 nm) absorption spectrum with good hyperchromicity in the absorption intensity. Upon sequential addition of Drew-AT (0, 1, 2, 3 and 4 μM), the absorption spectra of **QCy–DT** showed a gradual red shift in the absorption maxima (463 to 479 nm and 530 to 564 nm) with hyperchromicity (Figure 2A). **QCy–DT** experience hydrophobic environment upon binding to minor groove of AT-rich duplex DNA which prevents aromatic π-stacking interactions with base pairs and other molecules of the probe that led to the hyperchromicity in the absorbance maximum of **QCy–DT**. Remarkably, **QCy–DT** showed a ∼200-fold enhancement in the fluorescence emission at λ_{em} = 650 nm in the presence of Drew-AT with blue shift ($\Delta\lambda_{max}$ = ∼27 nm) compared to basal fluorescence of the probe alone (Figure 2B). Further, we studied the absorption and emission properties of **QCy–DT** in the presence of poly AT- and GC-duplexes. In the presence of $(A\text{-}T)_{20}$, **QCy–DT** showed red shift in the absorption maxima with hyperchromicity similar to that of Drew-AT (Supplementary Figure S4A). **QCy–DT** exhibited only a slight red shift in the absorption maxima at 463 and 530 nm in the presence of $(G\text{-}C)_{20}$, $(D1)_{mix}$ and $d(ATAT)_5$ (Supplementary Figure S4B–S4D). Interestingly, **QCy–DT** showed almost ∼250-fold fluorescence enhancement for $(A\text{-}T)_{20}$, compared to the only 8-fold increase observed for $(G\text{-}C)_{20}$ duplex (Supplementary Figure S5A). Further, we also studied the emission behavior of **QCy–DT** in presence of CT-DNA, $(D1)_{mix}$, single-stranded (ss) DNAs and RNA. In CT-DNA, $(D1)_{mix}$ and ssDNAs exhibited ∼40, ∼55 and ∼2-fold enhancements, respectively. Fluorescence spectra showed a very weak response of **QCy–DT** in presence of RNA that confirmed selectivity of the probe for DNA duplexes containing AT-base pairs (Supplementary Figure S5B). To ascertain the switch-on behavior of **QCy–DT** in the presence of AT-rich DNA duplex, we performed viscosity measurements by increasing the glycerol content in buffer solution (30). With increasing glycerol content, fluorescence spectra of **QCy–DT** exhibited a gradual enhancement in the emission intensity at 680 nm (Supplementary Figure S6). This tendency of the probe to have increased emission intensity with an increase in the glycerol content clearly suggests that the restriction of intramolecular rotation is responsible for the fluorescence enhancement of **QCy–DT**. Consequently, the observed strong fluorescence enhancement in the presence of AT-rich DNA duplexes is the result of restriction of intramolecular rotation of probe **QCy–DT** in the constrained environments of DNA, which also facilitates the desolvation (water molecules) around **QCy–DT** in the hydrophobic environment of DNA duplex (Figure 1C) (10,46,47). These preliminary results, thus, confirmed switch-on NIR-fluorescence behavior of **QCy–DT** in the presence of AT-rich DNA duplexes compared to that of GC-rich DNA duplex, ssDNAs and RNA.

Base pair-specific recognition and switch-on fluorescence in the presence of DNA

To gain deeper insights into base pair selectivity of the probe, we performed comparative and base pair-dependent fluorescence measurement in the presence of $(A\text{-}T)_{20}$, $d(ATAT)_5$, Drew-AT, $(D1)_{mix}$ and $(G\text{-}C)_{20}$ duplexes with 20, 6, 4 and 0 sets of AT-base pairs, respectively. We observed ∼8, ∼55, ∼54, ∼200 and ∼250-folds fluorescence enhancement in the presence of $(G\text{-}C)_{20}$, $(D1)_{mix}$, $d(ATAT)_5$, Drew-AT and $(A\text{-}T)_{20}$ with increasing number of AT-base pairs, respectively (Figure 3). Further, we carried out concentration-dependent studies with $(A\text{-}T)_{20}$ and Drew-AT duplexes by adding increasing concentrations of **QCy–DT**. With increasing concentration of **QCy–DT** (0–8 μM) to $(A\text{-}T)_{20}$ duplex, the fluorescence intensity gradually increased at 650 nm and attained saturation at ≥6 μM (Supplementary Figure S7). Similar spectral changes were observed for **QCy–DT** in the presence of Drew-AT (Figure 2C). We also recorded the fluorescence spectra of **QCy–DT** with increasing concentrations of $(A\text{-}T)_{20}$, Drew-AT, $d(ATAT)_5$ and $(D1)_{mix}$ duplexes. Figure 2D shows a gradual increase in fluorescence with increasing concentration of Drew–AT from 0 to 2 μM and saturation ≥2 μM.

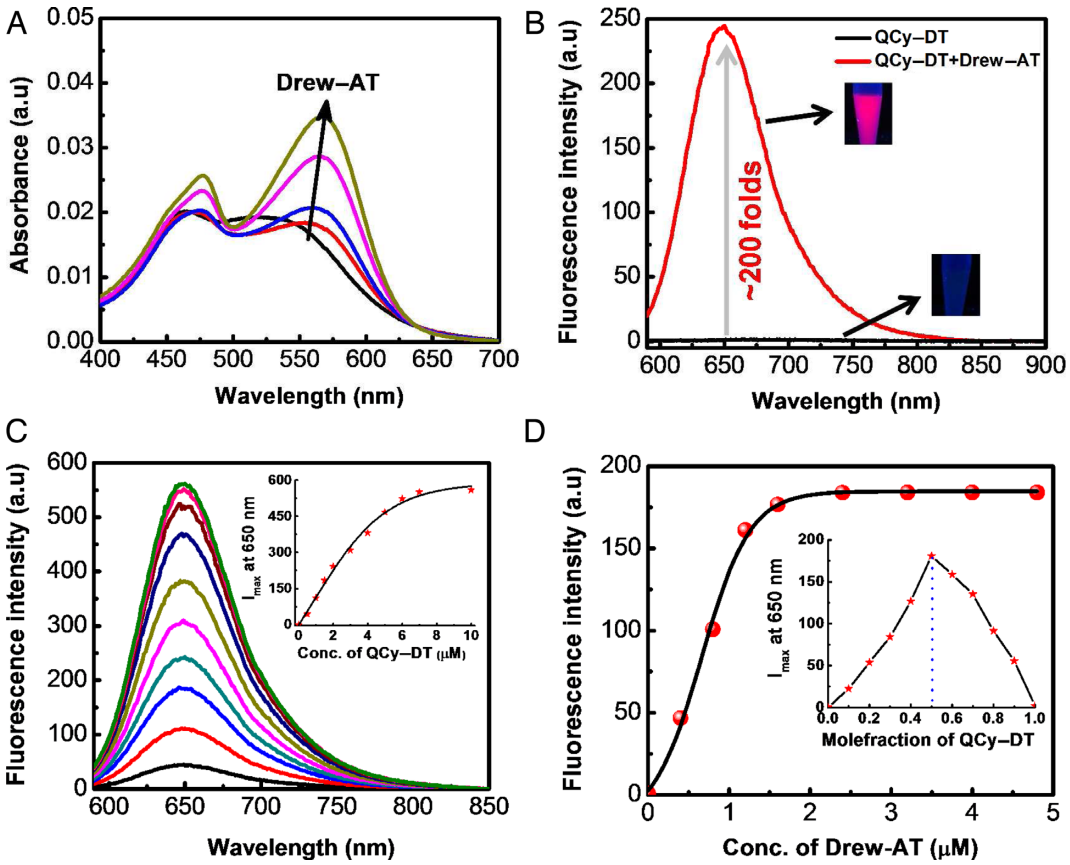

Figure 2. Photophysical properties of **QCy–DT**. (**A**) Absorption spectra of **QCy–DT** (2 μM) with increasing concentration of Drew–AT (0, 1, 2, 3 and 4 μM). (**B**) Fluorescence spectrum of **QCy–DT** (2 μM) in the presence of Drew–AT (4 μM). (**C**) Fluorescence spectra of Drew–AT (4 μM) with increasing concentration of **QCy–DT** (0–10 μM), *Inset*: Shows the plot of fluorescence intensity as a function of the concentration of **QCy–DT**. (**D**) Fluorescence titration curve of **QCy–DT** with increasing concentration of Drew–AT (0–5 μM). *Inset*: Job plot of **QCy–DT** with Drew–AT, which show 1:1 binding stoichiometry.

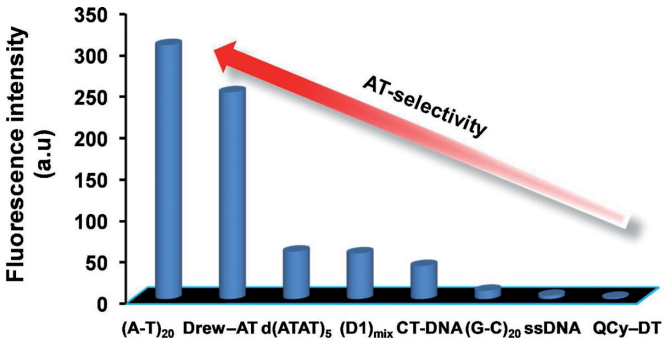

Figure 3. Base pair-dependent recognition of AT-rich DNA by **QCy–DT**.

Upon increasing concentration of other duplexes $(A\text{-}T)_{20}$, $d(ATAT)_5$ and $(D1)_{mix}$, **QCy–DT** showed similar fluorescence enhancement (Supplementary Figure S8). Overall, the strong fluorescence enhancements suggest **QCy–DT** is a selective and NIR-fluorescence-ready probe for DNA containing AT-base pairs (Figure 3).

Binding stoichiometry, affinity and quantum yield of QCy–DT for DNA duplexes

To determine the binding stoichiometry of **QCy–DT** with Drew–AT, we employed the continuous variation method, varying the ligand concentrations to generate the Job plot by fixing the total concentration of [**QCy–DT**+Drew–AT] at 2 μM (48). The Job plot analysis showed maximum fluorescence at 0.5, indicating 1:1 binding stoichiometry for the [**QCy–DT**:Drew–AT] complex (Figure 2D, *Inset*). We calculated the binding constants of [**QCy–DT**+DNA] complexes from the fluorescence titration experiments using non-linear (single-binding mode) curve fitting analysis (49). **QCy–DT** showed the maximum binding affinity ($K_a = 2.9 \times 10^6\ M^{-1}$) for $(A\text{-}T)_{20}$, which is 2-fold higher than that for Drew–AT ($K_a = 1.5 \times 10^6\ M^{-1}$). The mixed sequence $(D1)_{mix}$ showed relatively weaker binding affinity ($K_a = 4.3 \times 10^5\ M^{-1}$) compared to AT-rich DNA duplexes (Supplementary Figure S9). Next, we estimated the fluorescence quantum yield of **QCy–DT** in the presence of AT- and GC-rich DNA duplexes (supplementary Table S3). **QCy–DT** alone showed very low fluorescence quantum yield ($\Phi_F = \sim 0.004$) and increased significantly in the presence of glycerol ($\Phi_F = \sim 0.07$). Remarkably, **QCy–DT** showed maximum fluorescence quantum yield in the presence of $(A\text{-}T)_{20}$

(Φ_F = ~0.32) and Drew–AT (Φ_F = ~0.25) compared to other duplexes used in our study (supplementary Table S2). The quantum yield values of **QCy–DT** in the presence of AT-rich DNA duplex are comparable to commonly employed fluorescence probes (30). To understand the effect of **QCy–DT** binding to DNA on the thermal stability of DNA, we performed temperature-dependent UV-melting studies (UV-T_m) on different [**QCy–DT**+DNA] complexes. The UV-T_m studies of **QCy–DT**-bound $(A\text{-}T)_{20}$, Drew–AT, $d(ATAT)_5$ and $(D1)_{mix}$ showed increase in melting temperatures (T_m) with ΔT_m = 6.2, 4.2, 3.5 and 2.5°C, respectively (supplementary Table S4). The T_m data showed moderate stabilization of DNA duplexes in the presence of **QCy–DT**. Therefore, the binding affinty, fluorescence quantum yield, and UV-T_m data validated the preferential recognition of AT-rich DNA by **QCy–DT** probe compared to GC-rich DNA.

Mode of AT-rich DNA recognition by QCy–DT

To determine the binding mode of **QCy–DT** to AT-rich $(A\text{-}T)_{20}$ and Drew–AT DNA duplexes, circular dichroism (CD) studies were carried out under ambient conditions. CD spectrum of $(A\text{-}T)_{20}$ alone showed a positive and a negative signal at 280 and 248 nm, respectively. Similarly, Drew–AT showed a positive and a negative signal at 280 and 250 nm, respectively. These characteristic positive and negative CD signals confirm the typical B-form DNA duplex structure (50,51). At this point, two binding modes intercalation and minor groove binding are expected for **QCy–DT** binding to DNA. From the CD data, we can distinguish between these modes by means of induced CD signal for the guest (probe) to confirm groove binding over intercalation. Keeping this in mind, interactions between **QCy–DT** and DNA could be monitored by induced CD signals in the >300 nm region that gives information about the chiral environment around the probe on DNA. The concentration-dependent CD spectra recorded by the addition of increased concentrations of **QCy–DT** (0–16 μM) to fixed concentration of $(A\text{-}T)_{20}$ (4 μM) showed strong induced positive CD signals at 575 and 366 nm and a negative signal at 476 nm in the absorption regions of **QCy–DT** (Figure 4A). Similarly, we observed induced CD signals for **QCy–DT** in the presence of Drew–AT, though with relatively low intensity (Figure 4B). Thus, characteristic induced CD signal in the **QCy–DT** absorption region revealed that the probe bound to the minor groove of AT-rich DNA duplexes (51).

Furthermore, we performed *ab initio* theoretical calculations to unravel various features of **QCy–DT**/DNA interaction using DFT methods. Two possible modes (intercalation and groove binding) were considered for the binding of the bent **QCy–DT** to duplex DNA. The DNA phosphate backbone was neutralized by adding hydrogen to one of the oxygen atoms of the phosphate groups that would not alter any property of the duplex DNA structure (52,53). To calculate the binding energies of **QCy–DT** with DNA, we chose AT- and GC-rich duplexes (A/T and G/C) for each of these modes (supplementary Table S5). Our computed binding energy values confirm that **QCy–DT** prefers to bind in the minor groove of duplex DNA irrespective of the sequences. An inspection of the binding energy table re-

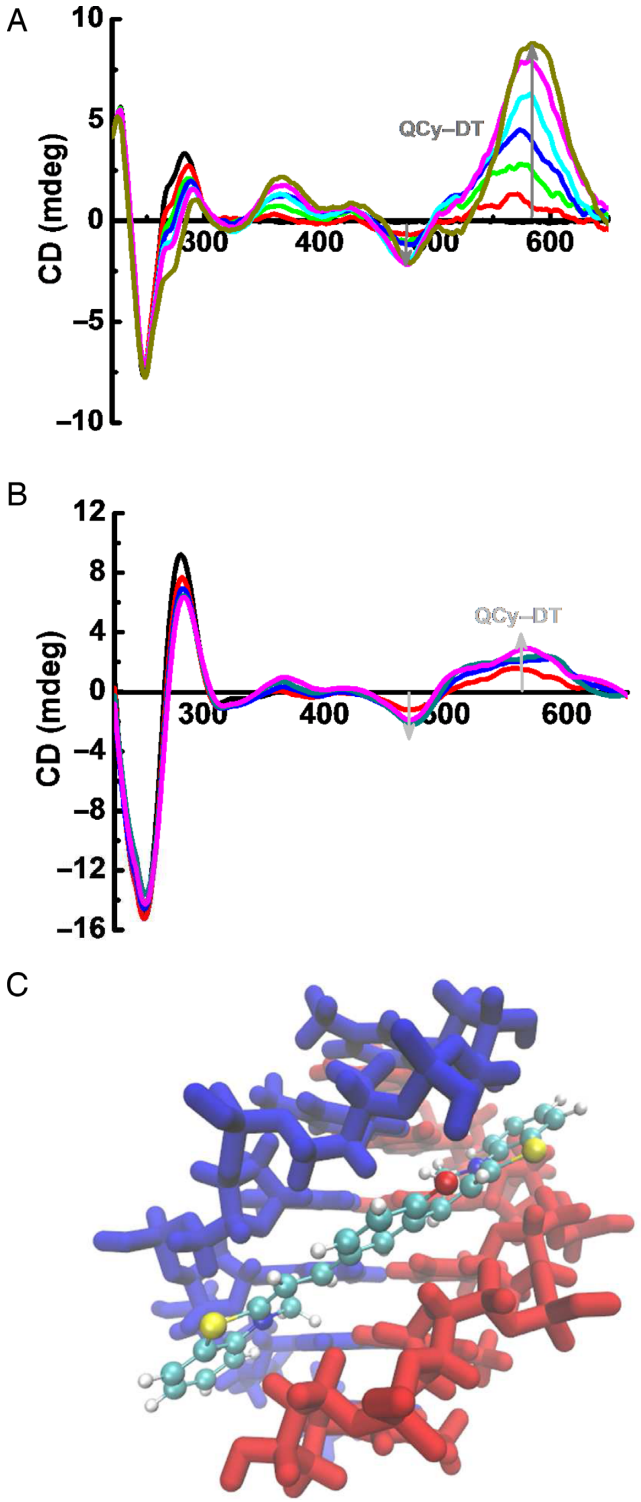

Figure 4. Circular dichroism (CD) spectra of **QCy–DT** in the presence of AT-rich DNA duplexes and view of minor groove binding mode of **QCy–DT**. (**A**) and (**B**) CD spectra of $(A\text{-}T)_{20}$ (4 μM) and Drew-AT (4 μM) with increasing concentration of **QCy–DT** from 0 to 16 μM, respectively. (**C**) Geometry optimized structure of the AT-rich DNA complexed with **QCy–DT** in the minor groove.

veals that the probe binds more strongly to AT-base pair (−105 to −110 kcal/mol) compared to GC-base pair (−85 to −90 kcal/mol) containing duplexes. It is known that minor groove of AT-rich duplexes is narrower than minor-groove of GC-rich duplexes (10). Thus, **QCy–DT** is found to be better accommodating in the minor groove of AT-rich DNA than GC-rich ones, which is apparent from the binding energy values (Figure 4C). Generally, the floor of minor groove with AT-base pairs has the highest negative electrostatic potentials while GC-base pairs possess the highest positive potentials. Naturally, the positively charged **QCy–DT** prefers to bind in the AT-rich minor grooves of DNA compared to minor groove consisting of GC-base pairs. In our calculations, we considered two possible orientations of **QCy–DT** in the minor groove of AT-base pair containing DNA, and the cationic quaternary nitrogen centres of the molecule can be located either (i) inside or (ii) outside of the groove. In this respect, binding energy values suggest that the former orientation where the cationic centres are arranged inside the minor groove of DNA are stabilized by −35 kcal/mol more than the latter. These results support the early reported literature that the positively charged surface of the molecule always projects toward the minor groove of DNA. Snapshots of the optimization process of 5′-AAATTT-3′/**QCy–DT** complex are shown in Supplementary Figure S10. Overall, computational results are well-corroborated with the experimental data that **QCy–DT** prefers to bind in the minor groove, with a preference for AT-base pairs over GC-base pair containing DNA.

Sequence-specific recognition of DNA by QCy–DT

Surprisingly, we noticed almost ∼4-folds difference in fluorescence enhancement of **QCy–DT** in the presence of $(A\text{-}T)_{20}$ compared to self-complementary, alternative AT-base pair containing $d(ATAT)_5$ duplex, although both contain total 20 AT base pairs (Figure 3 and Supplementary Figure S5A). This finding hinted at the highly sequence-specific recognition ability of **QCy–DT** for a specific combination of AT-base pairs in DNA duplex. As per our knowledge, there are no NIR-fluorescence probes that sequence-specifically recognize the minor groove of AT-rich DNA. The possible sequence-selectivity among AT-base pairs and the typical length of the bent shaped **QCy–DT** encouraged us to investigate its ability to bind with a specific combination of AT-sequence with a sequence length of four base pairs. For this purpose, we designed four DNA duplexes with variable $(A/T)_4$ base pairs such as 5′-ATAT-3′ (DM1), 5′-ATTA-3′ (DM2), 5′-AAAA-3′ (DM3) and 5′-AATT-3′ (DM4) at the central core (Figure 5A) (54). **QCy–DT** showed ∼8, ∼15, ∼40 and ∼72-folds fluorescence enhancement in the presence of DM1, DM2, DM3 and DM4 with 5′-ATAT-3′, 5′-ATTA-3′, 5′-AAAA-3′ and 5′-AATT-3′ core sequences, respectively, with promising blue shift ($\Delta\lambda_{max}$ = ∼32 nm) in fluorescence maxima (Figure 5B and Supplementary Figure S11A). Interestingly, **QCy–DT** showed the highest and lowest fluorescence enhancement in the presence of DM4 (5′-AATT-3′) and DM1 (5′-ATAT-3′), respectively. It is well known that most of the minor groove binders like netropsin, distamycin, Hoechst (bisimidazole dyes) and phenyl-furan-benzimidazole diamidine derivatives have the

A

Code	Central DNA core (B4)	Code	Central DNA core (B6)
DM1	5′-ATAT-3′	Drew–AT	5′-AAATTT-3′
DM2	5′-ATTA-3′	DM5	5′-TAATTA-3′
DM3	5′-AAAA-3′	DM6	5′-CAATTG-3′
DM4	5′-AATT-3′	DM7	5′-GAATTC-3′

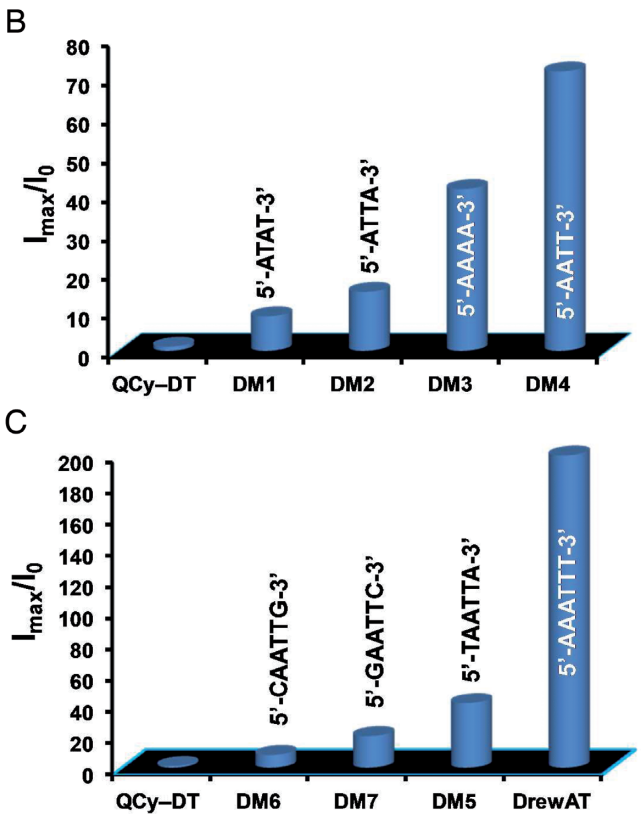

Figure 5. Sequence-specific recognition of AT-rich DNA minor groove by **QCy–DT**. (**A**) Table comprises the DNA sequences used in this study and DNA-sequence represents the following sequence of 5′-GCGC-Bn-GCGC-3′, where B is nucleobase with n = 4, 6 is AT-rich central core. (**B**) Plot of fluorescence intensity of **QCy–DT** ratio against the variable (A/T)4 sequence. (**C**) Plot of fluorescence intensity ratio of **QCy–DT** against local variations around 5′-X(AATT)Y-3′ sequences.

ability to recognize variable $(A/T)_4$ base pairs. Here, 'minor groove width' is one of the key parameters that dictate the sequence-selective binding ability of small molecules in the presence of variable (A/T)-rich sequences, depending on their base pair roll (55,56). Among all the variable $(A/T)_4$-sequences, 5′-AATT-3′ and 5′-ATAT-3′ are the two sequences that exhibit narrower and wider minor groove width with zero and large base pair roll, respectively (57,58). Therefore, we correlate that our probe **QCy–DT** recognizes the narrow minor groove width of 5′-AATT-3′ sequence in a DNA duplex, which favors fluorescence enhancement through the restriction of intramolecular rotation of **QCy–DT** compared to the relatively wider groove of 5′-ATAT-3′

sequence. These results clearly establish the high sequence sensitivity of the probe **QCy–DT** to the variation of $(A/T)_4$ base pairs as the width and interactions vary in the minor groove. This study established the sequence-specificity of **QCy–DT** in recognizing AT-rich DNA duplex minor groove containing 5′-AATT-3′ sequence.

To understand finer details of the interactions of **QCy–DT** with local variations around 5′-AATT-3′ sequence in the minor groove of DNA duplex, we performed fluorescence studies in the presence of DNA containing core hexanucleotide sequences such as 5′-*X*(AATT)*Y*-3′ (where *X* = *A*/*T*/*G*/*C* and *Y* is complementary base of *X*) (Figure 5A). **QCy–DT**, in the presence of DNAs containing 5′-*G*AATT*C*-3′ and 5′-*C*AATT*G*-3′ cores, showed very weak fluorescence enhancement. Remarkably, enormous fluorescence enhancement was observed in the presence of DNA with 5′-*A*AATT*T*-3′ core, which was ∼4-folds higher than the DNA with 5′-*AATT*-3′ core sequence alone. Surprisingly, replacing *A* with *T* at *X* in 5′-*X*(*AATT*)*Y*-3′ sequence reduced the fluorescence enhancement of **QCy–DT**, which was ∼1.5-folds lesser than 5′-AATT-3′ sequence (Figure 5C and Supplementary Figure S11B). To validate these findings, we carried out extensive computational calculations using DFT with localized basis (see supplementary data for computational details) to find that optical transitions in these systems occur between two states where charges are transferred from the DNA double helix to the bound molecule in the minor groove. In the case of **QCy–DT** binding to 5′-*A*AATT*T*-3′, the emission is dictated by complete charge transfer from the first adenine to the bound molecule, forming a strong dipolar matrix. For the 5′-*T*AATT*A*-3′, the first thymine does not contribute to the emission. However, in the latter case, the optical transition results into two states with weak transition dipoles, thereby giving broad emission spectra (Supplementary Figures S12 and S13).

Fluorescence imaging, cytotoxicity studies and photostability of Probe QCy–DT

Sequence-specific recognition of AT-rich DNA minor groove by switch-on NIR-fluorescence of **QCy–DT** encouraged us to further study its cellular uptake and applications in nuclear DNA staining. In order to check its permeability, we carried out cellular uptake studies in live and fixed conditions of MCF-7 and HeLa cells, respectively. First, MCF-7 cells were incubated with probe **QCy–DT** (0.5 and 1 μM) without fixing, and live cell imaging was conducted using Carl Zeiss fluorescence microscope. Fluorescence imaging of MCF-7 cells with **QCy–DT** showed selective staining of the cell nucleus by the probe, suggesting that **QCy–DT** is cell membrane-permeable molecule that confers selective staining of the nucleus (Figure 6A–D and Supplementary Figure S14A–S14D). Next, we fixed HeLa cells and incubated with **QCy–DT** (0.5 and 1 μM) along with Hoechst as the control nuclear staining dye. Fluorescence images showed selective staining of the cell nucleus, and remarkable co-localization with Hoechst dye (Figure 6E–H and Supplementary Figure S14E–S14H). Further, cells showed the pattern of black nucleoli, which is a characteristic feature of specific DNA minor groove binders over single-strand DNA and RNAs (59). Therefore, staining results obtained with live and fixed cells confirmed high cell permeability, efficiency (low staining concentration of 1 μM), and preferential targeting of cell nuclear DNA. Cytotoxicity is a major constraint with several DNA binding probes. To investigate the cytotoxicity of **QCy–DT**, we performed cell viability assay (MTT assay) in MCF-7 cells after incubation of 72 h. It was observed that up to 8 μM of **QCy–DT,** >76% cell viability was retained over a treatment period of more than 72 h (Supplementary Figure S15A) suggesting low-toxicity of **QCy–DT.** Another important criterion for a fluorescent molecule to be used as a probe for cell imaging applications is its stability upon excitation (60). To evaluate whether the cells could sustain the excitation of an argon ion laser and still provide a fluorescent signal bright enough for cell imaging, photostability assay was performed for **QCy–DT** in MCF-7 cells. After continuous 120-second argon ion laser excitation at 568 nm, **QCy–DT** exhibited a remainder fluorescence intensity of ∼80%. Also, ∼ 50% fluorescent signal intensity could be detected even after 300 s excitation (Supplementary Figure S15B). Overall, cell staining and viability assays confirmed the low-toxicity, cell permeability, photostability and selective nuclear targeting ability of **QCy–DT**.

Selective staining of *Plasmodium falciparum* nucleus and toxicity to malaria parasites by minor groove binding ligand QCy–DT

We selected *Plasmodium falciparum* as a model system to confirm the selectivity of probe **QCy–DT** toward AT-rich dsDNA in a cellular environment as the malarial parasite possesses a genome exceptionally rich in AT-base pairs (∼80%). It will also help us to determine whether **QCy–DT** has any detrimental effect on Plasmodium parasites. The parasites were incubated with 0.5 μM concentration of probe **QCy–DT** at early trophozoite stage. Live fluorescence imaging of these parasites showed that probe **QCy–DT** could specifically stain the parasite nuclei, but not the cytosolic part of the parasite or red blood cells (RBC) (Figure 7A–D). These results clearly indicate that probe **QCy–DT** binds to the AT-rich genome of the parasite at low concentrations. Also, uptake by malaria parasites and specific enrichment of the probe **QCy–DT** within the nucleus of the parasites indicate the possibility of the molecule's potential to interfere with the DNA metabolism of *P. falciparum*. Minor groove binding ligands like distamycin A, netropsin, 4'-6-diamidino-2- phenylindole (DAPI) and bisbenzimide (Hoechst 33258) have been known to inhibit the growth and propagation of *Plasmodium falciparum* in culture (61). Therefore, we were interested in assessing the inhibitory action of **QCy–DT** in malarial parasites. To assess this, IC_{50} of the probe **QCy–DT** was determined by treating early trophozoite stage *P. falciparum* (when DNA replication initiates) and the parasites were followed for the next cycle when new rings are formed. IC_{50} for **QCy–DT** against *P. falciparum* parasites was found to be <4 μM (Figure 7E), similar to netropsin. It was observed that parasites were arrested in the trophozoite stage and could not form rings in the following cycle at a higher concentration of 8 μM (data not shown). The arrest of the cells during trophozoite stage

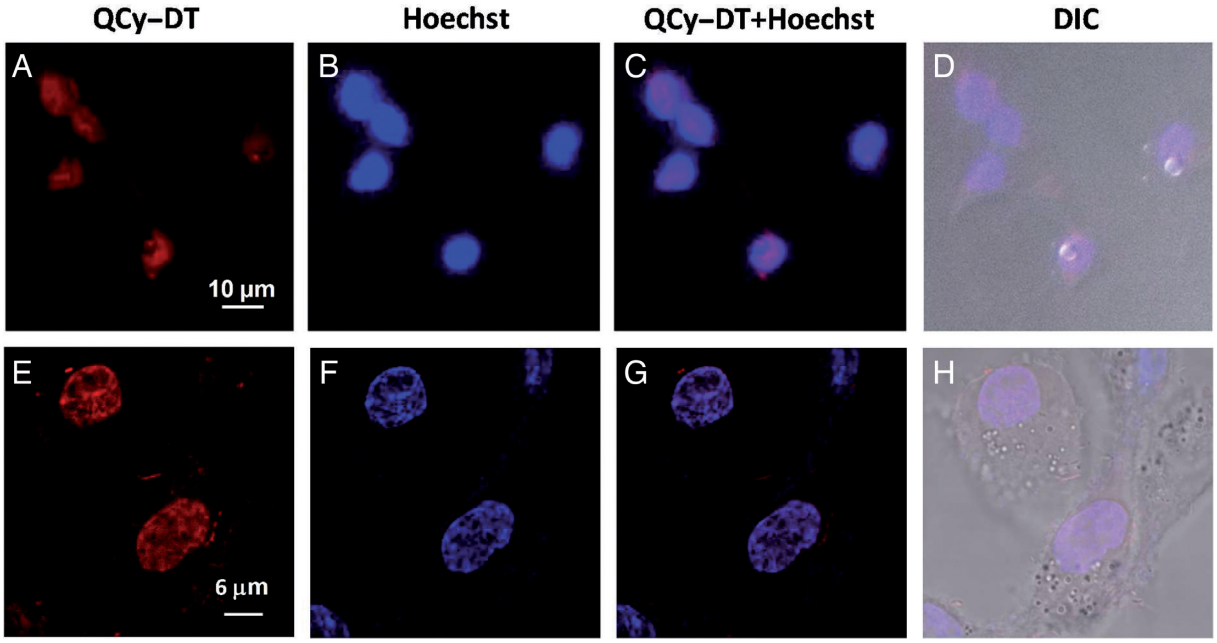

Figure 6. Cellular uptake properties of **QCy–DT** in live MCF-7 and fixed HeLa cells. (**A**–**D**) Fluorescence microscope images of live MCF-7 cells incubated with **QCy–DT**. (**A**) **QCy–DT** (0.5 μM), (**B**) Hoechst (0.5 μM), (**C**) overlay image of (**A**) and (**B**), (**D**) differential interference contrast (DIC, bright field image) with overlay of (**A**) and (**B**). (**E**–**H**) Confocal microscope images of fixed HeLa cells incubated with **QCy–DT**. (**E**) **QCy–DT** (0.5 μM), (**F**) Hoechst (0.5 μM), (**G**) overlay image of (**E**) and (**F**), (**H**) differential interference contrast (DIC, bright field image) with overlay of (**E**) and (**F**). Images were collected from 600–800 nm upon excitation at 520 nm.

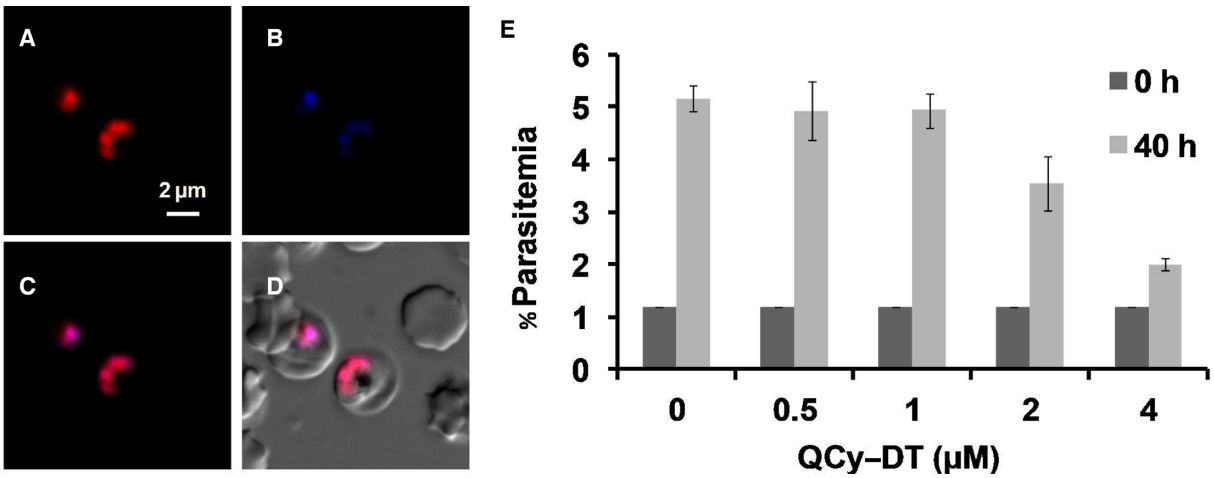

Figure 7. Uptake of **QCy–DT** in live *Plasmodium falciparum* parasites. (**A**–**D**) Fluorescence microscope images of blood stages of *Plasmodium falciparum* incubated with **QCy–DT**. (**A**) **QCy–DT** (0.5 μM), (**B**) DAPI, (**C**) Overlay of images of (**A**) and (**B**), (**D**) differential interference contrast (DIC, bright field image) with overlay of (**A**) and (**B**). Fluorescence images were collected from 600–720 nm upon excitation at 520 nm. (**E**) IC_{50} determination of **QCy–DT** in malaria parasites. A concentration range of 0, 0.5, 1, 2 and 4 μM of **QCy–DT** was used. The graphs were plotted for the percentage of parasitemia [at the beginning of the experiment, 0 h (∼20 h; early trophozoite stage parasites) and following 40 h of incubation with **QCy–DT** when the control parasites have entered the next cycle of invasion] against **QCy–DT** concentration, with mean and standard error.

suggests that the uptake of **QCy–DT** in the parasite nucleus may abrogate the process of DNA replication.

CONCLUSION

In conclusion, we demonstrated the unique sequence-specific and minor groove recognition properties of a newly designed NIR fluorescence probe **QCy–DT** for AT-rich DNA. Probe **QCy–DT** belongs to a new class of D2A (one-donor-two-acceptor) fluorophore (**QCy7**) with a distinctive ICT process responsible for the NIR fluorescence. The inherent non-fluorescent behavior of **QCy–DT** in unbound-state and switch-on fluorescence in the bound-state makes it a versatile DNA probe. Fluorescence studies of **QCy–DT** demonstrated its selective fluorescence enhancement in the presence of AT-rich duplexes over GC-rich DNA, single-stranded DNA and RNA. Circular dichroism studies confirmed the selective minor groove recognition of

AT-rich DNA, which induces the characteristic CD signal to **QCy–DT**. Computational studies further supported the minor groove recognition of AT-rich DNA in which the positively charged edge of **QCy–DT** was located inside the minor groove of DNA. Fluorescence studies of variable $(A/T)_4$ base pairs containing DNA duplexes revealed sequence-specific fluorescence enhancement in the presence of 5′-AATT-3′. Furthermore, investigations on the local variations around 5′-*X*(AATT)*Y*-3′ confirmed that $X = A$ and $Y = T$ (i.e. 5′-*A*AATT*T*-3′) is the most preferred sequence for depicting maximum fluorescence enhancement of **QCy–DT**. To the best of our knowledge, **QCy–DT** is the first switch-on NIR fluorescence probe to recognize minor groove of AT-rich DNA in a sequence-specific manner. Confocal fluorescence imaging and cell viability studies of MCF-7 and HeLa cells showed effective cell permeability, low-toxicity and selective staining of nuclear DNA both in live and fixed cell lines. Selective nuclear staining of *P. falciparum* and inhibition of its growth and propagation by **QCy–DT**, possibly through targeting cellular DNA, indicates **QCy–DT** as a potential therapeutic agent against particular parasitic infections similar to other minor groove binders. Remarkably, the IC_{50} value for *Plasmodium* parasites (<4 μM) is considerably low when a majority of the mammalian cells (∼75%) are still viable at a concentration of 8 μM. It is possible that the parasite killing activity of **QCy–DT** over the mammalian cells under similar experimental conditions is due to relatively higher affinity of the molecule for a high AT-rich parasite genome that may affect parasite DNA metabolism at a concentration not affecting the mammalian cellular machinery significantly. We envision that ease of synthesis, switch-on NIR-fluorescence, large Stokes shift, cell permeability, low-toxicity, cell imaging of both live and fixed cells, and parasite staining makes our new probe **QCy–DT** practically viable, inexpensive and a superior DNA probe compared to commercially available dyes routinely used (supplementary Table S6). The chemical diversity of our probe also offers means to design new enzymatic or chemically triggered self-immolative theranostic prodrugs for abnormal cells. Currently, work is ongoing in this direction in our laboratory.

SUPPLEMENTARY DATA

Supplementary Data are available at NAR Online.

ACKNOWLEDGEMENT

Authors thank Prof C.N. R. Rao for constant support and encouragement.

FUNDING

JNCASR, Research grants from the Council of Scientific and Industrial Research (CSIR) [02(0128)/13/EMR-II]; Department of Biotechnology (DBT) [BT/PR10263/NNT/28/711/2013]; Govt. of India [ICMS-JNCASR] for awarding Sheikh Saqr Career Award Fellowship, Alexander von Humboldt Foundation, Germany for special equipment donation to T.G., S.K.D. and M.N. acknowledge DBT and UGC for financial support, and CSIR senior research fellowship to N.N.

Conflict of interest statement. None declared.

REFERENCES

1. Rohs,R., Jin,X., West,S.M., Joshi,R., Honig,B. and Mann,R.S. (2010) Origins of specificity in protein-DNA recognition. *Annu. Rev. Biochem.*, **79**, 233–269.
2. Rohs,R., West,S.M., Sosinsky,A., Liu,P., Mann,R.S. and Honig,B. (2009) The role of DNA shape in protein-DNA recognition. *Nature*, **461**, 1248–1253.
3. Ginsburg,H., Nissani,E., Krugliak,M. and Williamson,D.H. (1993) Selective toxicity to malaria parasites by non-intercalating ligands. *Mol. Biochem. Parasitol.*, **58**, 7–15.
4. Hurley,L.H. (2002) DNA and its associated processes as targets for cancer therapy. *Nat. Rev. Cancer.*, **2**, 188–200.
5. Balasubramanian,S., Hurley,L.H. and Neidle,S. (2011) Targeting G-quadruplexes in gene promoters: a novel anticancer strategy? *Nat. Rev. Drug Discov.*, **10**, 261–275.
6. Wilson,W.D., Tanious,F.A., Mathis,A., Tevis,D., Hall,J.E. and Boykin,D.W. (2008) Antiparasitic compounds that target DNA. *Biochimie*, **90**, 999–1014.
7. Lerman,L.S. (1961) Structural considerations in the interaction of DNA and acridines. *J. Mol. Biol.*, **3**, 18–30.
8. Waring,M.J. (1968) Drugs which affect the structure and function of DNA. *Nature*, **219**, 1320–1325.
9. White,S., Szewczyk,J.W., Turner,J.M., Baird,E.E. and Dervan,P.B. (1998) Recognition of the four Watson-Crick base pairs in the DNA minor groove by synthetic ligands. *Nature*, **391**, 468–471.
10. Neidle,S. (2001) DNA minor-groove recognition by small molecules. *Nat. Prod. Rep.*, **18**, 291–309.
11. Dervan,P.B. (2001) Molecular recognition of DNA by small molecules. *Bioorg. Med. Chem.*, **9**, 2215–2235.
12. Moore,M.H., Hunter,W.N., Destaintot,B.L. and Kennard,O. (1989) DNA-drug interactions. The crystal structure of d(CGATCG) complexed with daunomycin'. *J. Mol. Biol.*, **206**, 693–705.
13. Dervan,P.B. (1986) Design of sequence-specific DNA-binding molecules. *Science*, **232**, 464–471.
14. Wemmer,D.E. (2001) Ligands recognizing the minor groove of DNA: development and applications. *Biopolymers*, **52**, 197–211.
15. Belitsky,J.M., Leslie,S.J., Arora,P.S., Beerman,T.A. and Dervan,P.B. (2002) Cellular uptake of N-methylpyrrole/N-methylimidazole polyamide-dye conjugates. *Bioorg. Med. Chem.*, **10**, 3313–3318.
16. Edelson,B., Best,T., Olenyuk,B., Nickols,N., Doss,R., Foister,S., Heckel,A. and Dervan,P.B. (2004) Influence of structural variation on nuclear localization of DNA-binding polyamide-fluorophore conjugates. *Nucleic Acids Res.*, **32**, 2802–2818.
17. Tanious,F.A., Hamelberg,D., Bailly,C., Czarny,A., Boykin,D.W. and Wilson,W.D. (2004) DNA sequence dependent monomer-dimer binding modulation of asymmetric benzimidazole derivatives. *J. Am. Chem. Soc.*, **126**, 143–153.
18. Athri,P. and Wilson,W.D. (2009) Molecular dynamics of water-mediated interactions of a linear benzimidazole-biphenyl diamidine with the DNA minor groove. *J. Am. Chem. Soc.*, **131**, 7618–7625.
19. Wilson,W.D., Nguyen,B., Tanious,F.A., Mathis,A., Hall,J.E., Stephens,C.E. and Boykin,D.W. (2005) Dications that target the DNA minor groove: compound design and preparation, DNA interactions, cellular distribution and biological activity. *Curr. Med. Chem. Anticancer Agents.*, **5**, 389–408.
20. Mathis,A.M., Bridges,A.S., Ismail,M.A., Kumar,A., Francesconi,I., Anbazhagan,M., Hu,Q., Tanious,F.A., Wenzler,T., Saulter,J. *et al.* (2007) Diphenyl furans and aza analogs: effects of structural modification on in vitro activity, DNA binding, and accumulation and distribution in trypanosomes. *Antimicrob. Agents Chemother.*, **51**, 2801–2810.
21. Tang,C., Paul,A., Alam,M.P., Roy,B., Wilson,W.D. and Hecht,S.M. (2014) A Short DNA Sequence Confers Strong Bleomycin Binding to Hairpin DNAs. *J. Am. Chem. Soc.*, **136**, 13715–13726.
22. Paine,M.F., Wang,M.Z., Generaux,C.N., Boykin,D.W., Wilson,W.D., De Koning,H.P., Olson,C.A., Pohlig,G., Burri,C., Brun,R. *et al.* (2010) Diamidines for human African trypanosomiasis. *Curr. Opin. Investig. Drugs.*, **11**, 876–883.

23. Soeiro,M.N., de Castro,S.L., de Souza,E.M., Batista,D.G., Silva,C.F. and Boykin,D.W. (2008) Diamidine activity against trypanosomes: the state of the art. *Curr. Mol. Pharmacol.*, **1**, 151–161.
24. Hunt,R.A., Munde,M., Kumar,A., Ismail,M.A., Farahat,A.A., Arafa,R.K., Say,M., Batista-Parra,A., Tevis,D., Boykin,D.W. *et al.* (2011) Induced topological changes in DNA complexes: influence of DNA sequences and small molecule structures. *Nucleic Acids Res.*, **39**, 4265–4274.
25. Haugland,R.P., Spence,M.T.Z., Johnson,I.D. and Basey,A. (2005) *The Handbook: A Guide to Fluorescent Probes and Labeling Technologies*. 10th edn, Molecular Probes, Eugene, OR.
26. Lavis,L.D. and Raines,R.T. (2008) Bright ideas for chemical biology. *ACS Chem. Biol.*, **3**, 142–155.
27. Sinkeldam,R.W., Greco,N.J. and Tor,Y. (2010) Fluorescent analogs of biomolecular building blocks: design, properties, and applications. *Chem. Rev.*, **110**, 2579–619.
28. Crissman,H.A. and Hirons,G.T. (1994) Staining of DNA in live and fixed cells. *Methods Cell Biol.*, **41**, 195–209.
29. Gill,M.R., Garcia-Lara,J., Foster,S.J., Smythe,C., Battaglia,G. and Thomas,J.A. (2009) A ruthenium(II) polypyridyl complex for direct imaging of DNA structure in living cells. *Nat. Chem.*, **1**, 662–667.
30. Narayanaswamy,N., Kumar,M., Das,S., Sharma,R., Samanta,P.K., Pati,S.K., Dhar,S.K., Kundu,T.K. and Govindaraju,T. (2014) A thiazole coumarin (TC) turn-on fluorescence probe for AT-base pair detection and multipurpose applications in different biological systems. *Sci. Rep.*, **4**, 6476.
31. Pfeifer,G.P., You,Y.-H. and Besaratinia,A. (2005) Mutations induced by ultraviolet light. *Mutat. Res.*, **571**, 19–31.
32. Blum,G., von Degenfeld,G., Merchant,M.J., Blau,H.M. and Bogyo,M. (2007) Noninvasive optical imaging of cysteine protease activity using fluorescently quenched activity-based probes. *Nat. Chem. Biol.*, **3**, 668–677.
33. Yuan,L., Lin,W., Yang,Y. and Chen,H. (2012) A unique class of near-infrared functional fluorescent dyes with carboxylic-acid-modulated fluorescence ON/OFF switching: rational design, synthesis, optical properties, theoretical calculations, and applications for fluorescence imaging in living animals. *J. Am. Chem. Soc.*, **134**, 1200–1211.
34. Maity,D. and Govindaraju,T. (2013) A turn-on NIR fluorescence and colourimetric cyanine probe for monitoring the thiol content in serum and the glutathione reductase assisted glutathione redox process. *Org. Biomol. Chem.*, **11**, 2098–2104.
35. Maity,D., Raj,A., Samanta,P.K., Karthigeyan,D., Kundu,T.K., Pati,S.K. and Govindaraju,T. (2014) A probe for ratiometric near-infrared fluorescence and colorimetric hydrogen sulfide detection and imaging in live cells. *RSC Adv.*, **4**, 11147–11151.
36. Trager,W. and Jensen,J.B. (1976) Human malaria parasites in continuous culture. *Science*, **193**, 673–675.
37. Armitage,B.A. (2005) Cyanine dye-DNA interactions: intercalation, groove binding, and aggregation. *Top. Curr. Chem.*, **253**, 55–76.
38. Karton-Lifshin,N., Segal,E., Omer,L., Portnoy,M., Satchi-Fainaro,R. and Shabat,D. (2011) A unique paradigm for a Turn-ON near-infrared cyanine-based probe: noninvasive intravital optical imaging of hydrogen peroxide. *J. Am. Chem. Soc.*, **133**, 10960–10965.
39. Redy-Keisar,O., Kisin-Finfer,E., Ferber,S., Satchi-Fainaro,R. and Shabat,D. (2014) Synthesis and use of QCy7-derived modular probes for the detection and imaging of biologically relevant analytes. *Nat. Protoc.*, **9**, 27–36.
40. Gnaim,S. and Shabat,D. (2014) Quinone-methide species, a gateway to functional molecular systems: from self-immolative dendrimers to long-wavelength fluorescent dyes. *Acc. Chem. Res.*, **47**, 2970–2984.
41. Rye,H.S., Yue,S., Wemmer,D.E., Quesada,M.A., Haugland,R.P., Mathies,R.A. and Glazer,A.N. (1992) Stable fluorescent complexes of double-stranded DNA with bis-intercalating asymmetric cyanine dyes: properties and applications. *Nucleic Acids Res.*, **20**, 2803–2812.
42. Cosa,G., Focsaneanu,K.-S., McLean,J.R.N., McNamee,J.P. and Scaiano,J.C. (2001) Photophysical properties of fluorescent DNA-dyes bound to single- and double-stranded DNA in aqueous buffered solution. *Photochem. Photobiol.*, **73**, 585–599.
43. Silva,G.L., Ediz,V., Yaron,D. and Armitage,B.A. (2007) Experimental and computational investigation of unsymmetrical cyanine dyes: understanding torsionally responsive fluorogenic dyes. *J. Am. Chem. Soc.*, **129**, 5710–5718.
44. Adamo,C. and Barone,V. (1999) Toward reliable density functional methods without adjustable parameters: The PBE0 model. *J. Chem. Phys.*, **110**, 6158–6170.
45. Spink,N., Brown,D.G., Skelly,J.V. and Neidle,S. (1994) Sequence-dependent effects in drug-DNA interaction: the crystal structure of Hoechst 33258 bound to the $d(CGCAAATTTGCG)_2$ duplex. *Nucleic Acids Res.*, **22**, 1607–1612.
46. Nguyen,B., Neidle,S. and Wilson,W.D. (2009) A role for water molecules in DNA-ligand minor groove recognition. *Acc. Chem. Res.*, **42**, 11–21.
47. Zhu,X. and Schatz,G.C. (2012) Molecular dynamics study of the role of the spine of hydration in DNA A-tracts in determining nucleosome occupancy. *J. Phys. Chem. B*, **116**, 13672–13681.
48. Job,P. (1928) *Ann. Chim. (Paris)*, **9**, 113–203.
49. McGhee,J.D. and von Hippel,P.H. (1974) Theoretical aspects of DNA-protein interactions: co-operative and non-co-operative binding of large ligands to a one-dimensional homogeneous lattice. *J. Mol. Biol.*, **86**, 469–489.
50. Ardhammar,M., Norde´n,B. and Kurucsev,T. (2000) In: Berova,N, Nakanishi,K and Woody,RW (eds). *DNA–drug interactions. in Circular Dichroism: Principles and Applications*. John Wiley & Sons Inc, NY, pp. 741–768.
51. Garbett,N.C., Ragazzon,P.A. and Chaires,J.B. (2007) Circular dichroism to determine binding mode and affinity of ligand-DNA interactions. *Nat. Protoc.*, **2**, 3166–3172.
52. Samanta,P.K., Manna,A.K. and Pati,S.K. (2012) Structural, electronic, and optical properties of metallo base pairs in duplex DNA: a theoretical insight. *Chem. Asian. J.*, **7**, 2718–2728.
53. Samanta,P.K. and Pati,S.K. (2014) Structural and magnetic properties of a variety of transition metal incorporated DNA double helices. *Chem. Eur. J.*, **20**, 1760–1764.
54. Breusegem,S.Y., Clegg,R.M. and Loontiens,F.G. (2002) Base-sequence specificity of Hoechst 33258 and DAPI binding to five $(A/T)_4$ DNA sites with kinetic evidence for more than one high-affinity Hoechst 33258-AATT complex. *J. Mol. Biol.*, **315**, 1049–1061.
55. Packer,M.J. and Hunter,C.A. (1998) Sequence-dependent DNA structure: the role of the sugar-phosphate backbone. *J. Mol. Biol.*, **280**, 407–420.
56. Laughton,C. and Luisi,B. (1999) The mechanics of minor groove width variation in DNA, and its implications for the accommodation of ligands. *J. Mol. Biol.*, **288**, 953–963.
57. Soler-LoÂ pez,M., Malinina,L. and Subirana,J.A. (2000) Solvent organization in an oligonucleotide crystal. The structure of $d(GCGAATTCG)_2$ at atomic resolution. *J. Biol. Chem.*, **275**, 23034–23044.
58. Cheng,J.-W., Chou,S.-H., Salazar,M. and Reid,B.R. (1992) Solution structure of $[d(GCGTATACGC)]_2$. *J. Mol. Biol.*, **228**, 118–137.
59. Spitzer,G.M., Fuchs,J.E., Markt,P., Kirchmair,J., Wellenzohn,B., Langer,T. and Liedl,K.R. (2008) Sequence-specific positions of water molecules at the interface between DNA and minor groove binders. *Chemphyschem*, **9**, 2766−2771.
60. Song,G., Sun,Y., Liu,Y., Wang,X., Chen,M., Miao,F., Zhang,W., Yua,X. and Jin,J. (2014) Low molecular weight fluorescent probes with good photostability for imaging RNA-rich nucleolus and RNA in cytoplasm in living cells. *Biomaterials*, **35**, 2103–2112.
61. Turner,P.R. and Denny,W.A. (2000) The genome as a drug target: sequence specific minor groove binding ligands. *Curr. Drug Targets*, **1**, 1–14.